Scientia Iranica A (2021) 28(3), 1079–1095

Sharif University of Technology
Scientia Iranica
Transactions A: Civil Engineering
http://scientiairanica.sharif.edu

A novel method for implementation of corrosion-induced cracks in the finite element models of reinforced concrete structures

S. Fahimi[a], M.R. Zakerzadeh[a], M. Baghani[a,*], and K. Zandi[b]

a. *School of Mechanical Engineering, College of Engineering, University of Tehran, Tehran, Iran.*
b. *Department of Architecture and Civil Engineering, Chalmers University of Technology, Gothenburg, Sweden.*

Received 2 February 2019; received in revised form 16 November 2019; accepted 16 November 2020

KEYWORDS
Reinforced concrete;
Corrosion induced cracking;
Crack models;
Corrosion models;
Finite element analysis.

Abstract. Currently, there is a clear need for reliable procedures for condition assessment and service-life evaluation of existing infrastructures. Advanced 3D Nonlinear Finite Element (3D NLFE) analysis has proven to be capable of describing the behavior of reinforced concrete provided that detailed and appropriate condition assessment data are available. The present study aims to review and compare different procedures for coupling 3D NLFE analysis with condition assessment data to model corrosion induced cracking, and, consequently to find a method with better accuracy, less computational cost, and improved robustness. This paper introduces a new method for adding cracked elements directly to the finite element model, called Re-FEM. The force-displacement response, ultimate crack pattern, and failure mode from this model are compared with four other methods for a pull out test case on specimens under an accelerated corrosion process. Using this method, the force displacement response for the corroded specimens was overestimated by about 70%. However, the trend was promising and the failure mode and crack pattern were correct. Moreover, the analysis continued after the peak point in the force-displacement curve, which makes it possible to monitor the behavior of the specimen in the softening regime.

1. Introduction

Today, the anticipated environmental and economic cost of replacing aging building/infrastructure stock is immense and defies true quantification. In the case of a bridge infrastructure, the best estimates for the replacement of one million bridges in the EU27 and more than 600,000 bridges in the United States amount to €400 billion and $300 billion, respectively [1]. National budget priorities do not allow this level of funding; consequently, many infrastructures will be left structurally deficient if not properly assessed and maintained.

Devising the repair timeframe of infrastructures requires an accurate assessment of their current condition. Such a condition assessment includes (a) frequent data collection through inspection and (b) the use of reliable structural performance predictive models. While traditional data collection methods by human inspectors largely consist of intrusive, time-consuming and subjective measures, the next generation of effective and accurate data collection platforms combining terrestrial, satellite and airborne systems,

*. *Corresponding author. Tel.: +98 21 61119921*
E-mail addresses: sh.fahimi@ut.ac.ir (S. Fahimi); zakerzadeh@ut.ac.ir (M.R. Zakerzadeh); baghani@ut.ac.ir (M. Baghani); kamyab.zandi@chalmers.se (K. Zandi)

doi: 10.24200/sci.2020.52829.2903

are under development. An example of such advancements is the UNICA concept – Autonomous Non-Intrusive Condition Assessment – (further explained in [2]). Next generation data collection, enabling a repository of 4D (3D + time) condition assessment data, may leverage updating leaps in the condition assessment of infrastructures, only if they are coupled with structural performance predictive models. Thus, there is a growing demand for the development of advanced predictive tools that can leverage massive inspection data, such as cracking and spalling in reinforced concrete, for an accurate condition assessment and service life prediction of structures.

Different ideas have been used to avoid damage and crack propagation in materials, e.g., development of self-healing materials [3–7] and reinforced concrete [8–10]. These materials exhibit a nonlinear response that requires numerical tools. Advanced Non-Linear Finite Element (NLFE) analysis has proven to be capable of describing the behavior of reinforced concrete in a comprehensive way, provided appropriate crack models have been adopted [11,12]. Over the years, several crack models have been introduced, aiming to capture the nonlinear behavior of cracked concrete as a brittle heterogeneous material. Some of the major differences between these models were the use of prior knowledge about the cracking path and its properties, the dependence of the crack path on mesh boundaries, consideration of minor cracks as well as major ones, and the computation scheme. Nonetheless, most of the models are barely coupled with cracking data obtained by visual inspection; i.e., crack patterns and crack width documented in inspections are not directly introduced to NLFE analysis. Thus, a brief state of the-art review of crack models and their potential to enable coupling between NLFE analysis and inspection data are among the primary focal points of the present study.

Corrosion of steel reinforcements is the most common cause of deterioration in reinforced concrete structures [13]. The corrosion products occupy a larger volume and change the reinforcement-concrete interface, which results in cracks in the surrounding concrete cover [14] and weakens the bond between the reinforcement and concrete [15–17]. For a larger amount of corrosion penetrations, splitting stresses due to volume expansion may lead to cover spalling [18], which makes stirrups the primary source of confinement in the cross section [19]. As a result, the anchorage capacity of the structure is influenced by cover cracking [16], cover spalling [20], and the corrosion of stirrups [21].

These phenomena can be included in the NLFE analysis of reinforced concrete structures with varying degrees of detail. In the simplest approach, interaction between the steel reinforcements and concrete is modelled using a 1D bond-slip relation [22]. The level of corrosion affects the local bond slip properties during the analysis [23,24]. Using a predefined bond-slip constitutive model as input for the analysis does not always reproduce the inspected corrosion induced cracks. In an advanced method, the bond stress depends not only on the slip, but also on the radial expansion of the bars due to the corrosion [25]. Thus, the model can predict bond loss at the splitting failure or the yielding of the reinforcement. Moreover, the generated stresses due to the volume expansion of corrosion products [26], and stress relief due to the flow of corrosion products through cracks [27], are considered in this model. A review of the models accounting for corrosion induced cracking in Finite Element (FE) analysis, and the study of methods by which the inspection data of the surface cracks are directly incorporated in the NLFE analysis is another focal point of the present paper.

In summary, the goals of this work were: (a) to give a brief state-of-the-art review on models for implementation of visually inspected "cracks" and "corrosion-induced cracks" in the numerical analysis of reinforced concrete structures and (b) to compare different methods of coupling condition assessment data and NLFE analysis. While the first objective was realized by a thorough literature review, the second objective was achieved by carrying out a case study, comparing four methods of incorporating corrosion-induced cracks into the 3D Nonlinear Finite Element (3D NLFE) analysis. These methods are based on: (1) modification of the bond-slip relation using the approach developed by Lundgren et al. [22], (2) bond-corrosion models earlier developed by Lundgren [28] and later extended by Zandi Hanjari et al. [27], in which bond stress is affected by radial deformation as well as slip, (3) an innovative simulation scheme that allows for replication of the inspected corrosion-induced cracks in the simulation using a smeared crack approach, and (4) a discrete crack model with embedded crack elements. The four methods were utilized to model earlier tested pull out specimens that had been subjected to an accelerated corrosion process. Then, the force displacement response, ultimate crack pattern, and failure mode observed in each analysis were compared with those in the experiments.

2. Comparison of crack models in FE analysis

In this section, the crack models are chosen based on workability and novelty, and the primary focus is on the pros and cons of each model for numerical simulation of corrosion induced cracking problems.

In the *smeared crack model*, small cracks nucleate and link up at later stages of the loading phase to form one or more dominant cracks [29]. In contrast, the *discrete crack model* is used for simulation of initiation

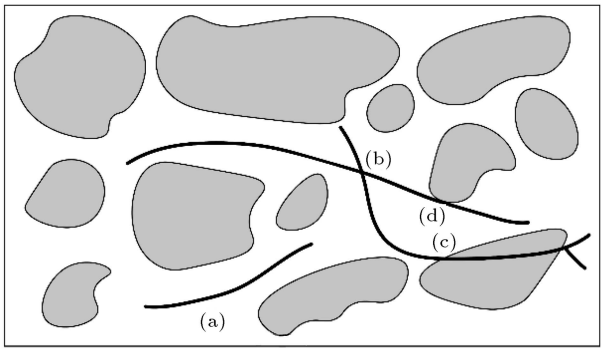

Figure 1. Crack propagation in heterogenic material, adopted from Van Mier [32].

and growth of dominant cracks [29]. The physics of crack initiation and growth in a heterogeneous quasi-brittle material, such as reinforced concrete, is illustrated in Figure 1. The presence of particles of different sizes and stiffnesses results in crack nucleation (a) and branching (b); these cracks may propagate across phase boundaries (c), or in interfaces (d). The nonlinear behavior of concrete in the cracking phase can also be estimated with acceptable accuracy by performing a sequence of linear analyses (*Sequentially Linear Analysis*), and scaling the strength of elements at each step accordingly [30]. If one enriches the elements or nodes with additional degrees of freedom, the cracking path will be independent of mesh boundaries [31]. *Embedded crack approaches* and the *extended finite element method (XFEM)*, both taking advantage of such additional degrees of freedom, are also reviewed and compared as examples of the meshless approaches. All these approaches are further discussed in the following sections.

2.1. The smeared crack approach

In a smeared crack approach, the initiation and growth of cracks in the volume attributed to an integration point are modeled by altering the stiffness and strength of the corresponding integration point [29]. Generally, a crack is initiated if the state of stress satisfies a specified criterion. While smeared crack approaches are particularly accurate in modeling different phases of cracking, the computational cost of this method is usually very high. Also, this approach is primarily developed for modeling crack growth and finding the final crack path, therefore, the numerical cost is not appropriate for studies focused on the response of a structure under loading with known crack paths.

The criterion that specifies the initiation of cracks is an important characteristic of smeared approaches. Various models are introduced considering different parameters as the crack identifier, such as decomposed strain based models [33], total strain based models [34], and plasticity based models [35]. The decomposition of the strain allows for the combination of cracking with other non-linear phenomena by e.g., decomposing the strain into an elastic part, a creep part, and a thermal part [33]. The difficulties of the decomposition of strain can be solved with simplified total strain-based models [34]. Total-strain based models are suitable for practicing engineers because there is no need to use abstract yield functions or sophisticated crack laws. Also, a unified approach for tension and compression can be obtained with a plasticity-based concept.

2.2. The discrete crack approach

The crack is introduced as part of the finite element mesh in the discrete crack approach. The crack will propagate if a predefined strength criterion is met at the crack tip. Then, the node at the tip of the crack will be split into two nodes and the crack tip will be propagated [36]. The same as the smeared crack approach, the criterion for crack development can be defined in different ways. Total relative displacement based relationship and plasticity based interface models are also examples of the discrete crack approaches [37].

Since the discrete cracks cannot propagate inside a continuum element, one significant disadvantage of this method is the dependency of crack propagation on element boundaries, which results in mesh bias. An automatic re meshing method, which generates a new mesh and transfers the data from the old mesh to the new one can reduce the mesh bias, with the drawback of an increase in the computational demand [29].

While the discrete crack approach is a suitable method to simulate a crack with a previously specified path, the simulation result is strongly dependent on the mesh geometry. Thus, implementing a complex crack geometry in the model is a difficult task, if not impossible, considering the available pre processing packages. Moreover, discrete crack models are susceptible to computational problems such as stress locking. Additionally, even though the approach allows for modeling of more than one crack, the increased number of interface elements will most definitely make the solution more complicated.

2.3. Sequentially Linear Analysis (SLA)

Sequentially Linear Analysis (SLA) [38] is an alternative to the non-linear finite element analysis of structures when bifurcation, complex snap-back [39] or divergence problems arise. In this approach, a series of scaled linear FE analyses are used instead of the incremental-iterative procedure in NLFE analysis [40]. In each linear analysis, a single point is selected with the highest utilization of its current strength properties. Then, the global load will be scaled according to the increased damage at this critical integration point. Applying increments of damage instead of force, displacement, arc-length or time, prevents large jumps in damage during a single time-step or load-step and

significantly improves the convergence. The damage increments are applied locally at integration points. Accordingly, compared with traditional methods, SLA is very effective in predicting localizations, crack spacing, and crack-width as well as brittle shear behavior. To use this model, the proportional loading assumption should be applicable. In proportional loadings, the principal stresses maintain constant directions and constant ratios of their values, while the load is changing with time.

Another ability of SLA is in solving perfectly symmetric problems, whereas in nonlinear finite element models, a finite load increment near peak will always initiate cracks in two symmetric integration points, simultaneously. However, in experiments, material imperfection triggers non symmetric solutions. In SLA, due to the scaling procedure, there is only one critical point at any time, thus, there is no need to add material imperfections.

While SLA is a robust solution, some limitations still exist. The inability to model crack closure and subsequent frictional sliding, long run-times for models with a large number of integration points, and deficiency in handling non-proportional loading are among the major shortcomings [41]. To date, this approach is available in few finite element packages and it is mostly used for verifying the result of nonlinear analyses.

2.4. Embedded crack models

In embedded crack approaches, the elements are enriched with additional degrees of freedom representing jumps in the displacements across the discontinuity; thus, the crack geometry is independent of the mesh boundaries. Introducing additional degrees of freedom can prevent the progress of crack because of kinematic incompatibility between the cracks in the neighboring elements [42]. Crack tracking procedures [43] can be used to re-establish the geometric continuity of the crack line and avoid this problem. Stress locking is also observed in standard embedded models, so employing a combined model is beneficial. In a combined model, the early stages of cracking are handled by smeared approaches and a discontinuity is implemented in later stages when the crack opens sufficiently wide.

While the implementation of this method is a straightforward procedure, the suitable element should be formulated in the desired finite element package. Also, this model can be viewed as a discrete model without the problem of mesh dependency, if it is employed after the crack formation. However, the problem of assigning correct material properties will remain.

2.5. Extended Finite Element Method (XFEM)

The Extended Finite Element Method (XFEM) enriches the standard interpolation function with a discontinuous part. In contrast to the elemental enrichment for elements with embedded discontinuities, the XFEM is based on nodal enrichment [44,45]. In XFEM, the model is divided into two distinct parts. The mesh will be generated in the geometric domain, and flaws and other geometric entities will be added by additional functions. This permits the incorporation of a prior knowledge about the problem characteristics and the corresponding solution.

While the computational cost of elemental enrichments (EFEM) is approximately independent of the number of cracks [45], the computational cost of XFEM is a linear function of the number of cracks. Eventually, both XFEM and EFEM converge to a similar result with the same convergence rate [45].

Because XFEM is based on nodal enrichments, it is a highly robust method for finite element analysis of cracking. However, the formulation of XFEM is cumbersome and the method is not implemented in many finite element packages. Today, almost all studies on XFEM are done using special packages formulated just for XFEM analysis and the geometries are not based on real-life scenarios.

The timeline of evolution and significant developments of the models, which are discussed in this paper, are shown in Figure 2. Other major models, that have influenced or been influenced by the models presented above, are also included in this figure. The dashed lines show the influence of one method on the improvement of another method which may have eventually created a new branch.

2.6. Implementation of crack models in commercial FEM packages

In Table 1, the availability of the above-mentioned models is shown in three well-known finite element packages for the analysis of reinforced concrete structures. In all three packages, users can implement user-defined materials and elements as well.

3. Modeling corrosion-induced cracks in FE analysis

Because corrosion is one of the major causes of cracking in reinforced concrete, there are plenty of studies covering the effect of this phenomenon on the behavior of structures. Bhargava et al. [46,47] modeled the

Table 1. Implementation of crack models in three common Finite Element (FE) software for crack modeling.

	Smeared	Discrete	SLA	XFEM
ABAQUS	Yes	Yes	No	Yes
ANSYS	Yes	Yes	No	Yes
DIANA	Yes	Yes	Yes	No

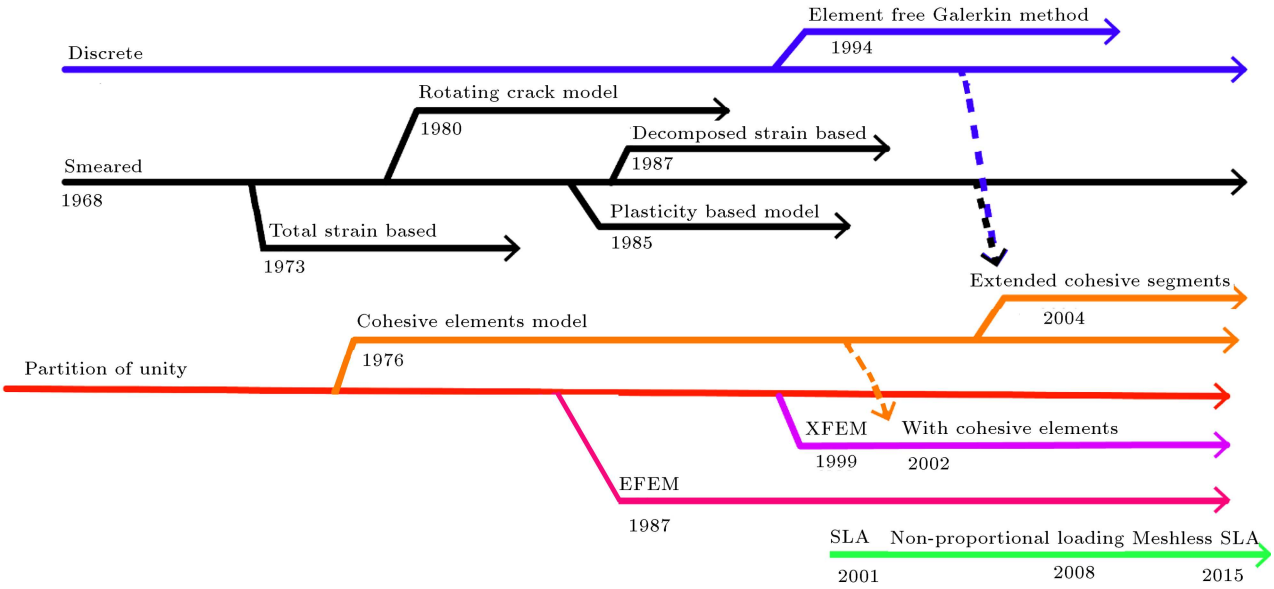

Figure 2. Evolution of crack models.

problem of concrete cover cracking and weight loss of reinforcement as a boundary value problem. They applied displacement boundary conditions to the internal surface of the steel-concrete interface to account for the corrosion products. The authors performed a sensitivity analysis and found that the tensile strength, the initial tangent modulus of the concrete, the annual mean corrosion rate, and the modulus of elasticity of reinforcement and corrosion products have a significant influence on the predicted time to cover cracking. Later, Wang et al. [48] showed that prestress can also accelerate the corrosion induced cracking process and decrease the time to cover cracking by changing the chemistry of corrosion products.

Another analytical model for corrosion-induced cracking in reinforced concrete structures is presented by Li et al. [49] based on fracture mechanics. They modelled a concrete bar with embedded reinforcement as a thick-walled cylinder. A parametric study by the authors on the effects of critical factors on corrosion-induced crack development, such as the corrosion rate, the geometry of specimens, and the mechanical properties of concrete, showed that the most important factor affecting both the crack width growth and the time to surface cracking is the corrosion rate. The authors also found that the geometry of the reinforced concrete represented by the cover to bar diameter ratio, and the concrete property represented by the tensile strength and the creep coefficient, affect the time to surface cracking more than crack width growth.

Val et al. [50] designed their study to investigate the amount of corrosion dissipation within the pores and cracks in concrete. Corrosion dissipation causes a reduction in the pressure exerted by the corrosion products on the surrounding concrete. The authors compared the results of the finite element model with the experimental data and concluded that the amount of corrosion penetration before crack initiation is larger than the simulation results. Also, they showed that corrosion fills the corrosion-induced cracks and concrete pores gradually over time. According to their test results, the time taken to fill a crack is directly related to the thickness of the concrete cover.

In 2010, Richard et al. [51] introduced a 3D formulation based on continuum damage mechanics for modeling the steel-concrete interface under corrosion. They avoided the use of classic contact elements by using degenerated elements in the numerical formulation. Guzmán et al. [52] used an embedded cohesive crack 2D finite element for simulating the cracking process. They showed that the proposed model can estimate the time to surface cracking accurately using some necessary assumptions on the mechanical properties of the rust, the corrosion rate, and the accommodation of corrosion products within the open cracks. Fracture models are also used to find crack width for uniform [53] and nonuniform corrosion distribution [54]. Mak et al. [55] showed that the surface crack widths are more accurate indicators of the bond degradation than the corrosion levels.

While most of the studies in corrosion-induced crack modeling consider a uniform corrosion distribution, where the expansion pressure is evenly distributed all around the rebar, non-uniform corrosion distribution represents the natural corrosion more accurately. Guzmán et al. [56] showed that the cracking pressure decreased by around 35–50% by considering non-uniform corrosion distribution around the rebar. They also found that the localization of crack happens at earlier stages, which shows that

assuming uniform corrosion overestimates the service life of concrete structures.

While different relations were introduced to model effects of corrosion on structural performance, most are focused on the same cause and effects and consider similar assumptions. Here, a model based on experimental data alongside an analytical model is introduced as major examples.

3.1. 1D-ARC approach

1D-ARC is a 1D model introduced by Lundgren et al. [22] as an extension of the 1D bond-slip model given in the CEB-FIP Model Code 1990 [57]. While the model can show the load-carrying capacity of a corroded structure, it is usually incapable of showing the correct failure type. It is an expected deficiency because this model is solely developed to produce a rough approximation of the bond capacity of the structure. It is also notable that while this model tends to underestimate structural strength in most scenarios, it is not the case for large corrosion penetrations or small amounts of transverse reinforcements.

3.2. Lundgren model

Lundgren [25] proposed a model to predict the behavior of the bond between the corroded specimen and concrete. In another work, Lundgren [28] employed the previously developed finite element model of corrosion with a bond mechanism model to study the effect of uniform and localized corrosion on reinforced concrete beams. It was observed that an axisymmetric model is sufficiently accurate for cover cracking due to uniform corrosion distribution, but for cases with localized corrosion, three dimensional models should be used.

In this model, special 2D elements are added at the interface to describe the relation between traction and relative displacement. Also, a frictional model is used to define the bond mechanism. The model applies to both the bond stress and the splitting stress. Modeling surrounding concrete makes it possible to obtain the splitting cracks or cone cracks near free edges.

To model the volume increase of corrosion products, a physical model is presented (Figure 3), in which the rust relative volume to the virgin steel and the corrosion penetration as a function of time are known. The free increase of the radius (the increase in radius under no normal pressure) is calculated using geometrical relations. Then, the normal pressure due to corrosion is determined by comparing the free increase of the radius to the actual radius of the bar.

As stated earlier, rust can fill the pores in concrete before applying pressure on the structure. This model accounts for the stress relief due to the flow of corrosion products by filling the pores in the crack-steel interface under zero stress and applying normal stresses to the surrounding concrete at the interface after filling the porosity.

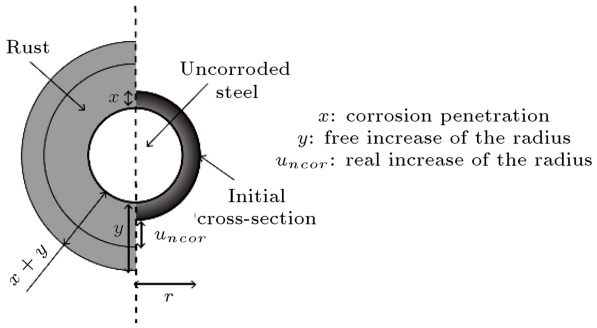

Figure 3. Physical interpretation of the variables in the corrosion model.

Zandi Hamjari et al. [27] extended Lundgren's corrosion model [28] to include the effect of corrosion products flowing through the cracks. They assumed a constant width for a crack through the depth, which results in a slight underestimation of the flow of corrosion products through cracks near the concrete surface. In Zandi's model, the volume flow of corrosion products depends on both the crack width and the pressure around the bar. The reduction in crack width is expected to delay numerical instability in the FE analysis. The analysis can thus be carried out for higher corrosion attacks. Moreover, since corrosion flow reduces the normal stress of the cracked elements, whilst maintaining the normal stress associated with other elements around the bar, other cracks can initiate and propagate, which results in a greater number of cracks with smaller crack width.

While the comprehensive models including corrosion flow, bond deterioration, and local corrosion can predict crack properties with good accuracy, the complex model demands high computational power. The required time for a full simulation of cracking could be significantly high for a small specimen. This is particularly important when the focus of research is on the behavior of a real-life cracked structure under loading. Another difficulty is associated with predicting secondary cracks. As the first crack initiates, many models are unable to accurately predict other tiny cracks around the rebar.

If the overall goal of one's work is to analyze the behavior of the cracked structure and check the possible options for assessment, a simplified method can be implemented to eliminate difficulties associated with modeling the cracking phase. In this method, the crack and deterioration of the structure are applied as a change in material properties near the cracked region and the constructed model will be used under the desired loading conditions. Since the model is a replicate of a real life specimen, the crack path and width are assumed to be known.

The above-mentioned method faces some issues.

First, the change of the material properties must be based on some parameters associated with the crack. The width and the path of the crack are two measurable parameters that can be used here. The crack path can be implemented in two different ways, either by changing the material properties of each element as an embedded characteristic or by defining new elements in a discrete crack manner. The crack softening curve presented by Cornelissen et al. [58] can be used as an empirical basis for changing the material properties based on the crack width measured in the experiments. Also, a method for altering bond properties after deterioration of the bond should be investigated. In the following section, a simple case will be presented to compare the weaknesses and strengths of different modeling approaches for corrosion induced cracking.

4. Case study of coupling condition assessment data of a pull out test and NLFE analysis

As a case study, to investigate the performance of different crack models, earlier tested pull-out specimens that have been subjected to an accelerated corrosion process were modeled using four different approaches:

1. **Adjusted 1D-ARC:** In the first approach, the effect of corrosion on the concrete-rebar interaction will be incorporated by adjusting the bond-slip relation using the 1D method developed by Lundgren et al. [22]. Using this approach, the bond will be deteriorated due to corrosion, but the corrosion induced cracks are not introduced in the geometry;
2. **3D bond corrosion:** In the second approach, the bond-corrosion model, developed by Lundgren [28] and later extended by Zandi et al. [27], will be used for the interface elements along with a separate corrosion phase. Using the bond-corrosion model, corrosion products exert pressure around the rebar and some cracks may develop in the first phase. After the pull-out phase, the structure force passive slip will be compared with the experimental results. Because of corrosion penetration and releasing pressure after crack development, the actual amount of corrosion is always more than the applicable amount of corrosion in the simulations. A pull-out phase should be modeled to compare the final force displacement results with experiments;
3. **Re-FEM:** In the third approach, which will be called Re-FEM in the rest of this paper, corrosion induced cracks will be introduced to the structure. Therefore, prior knowledge of the crack pattern and crack width is necessary for this approach. The crack path can be discretized to a series of points and the cracked elements can be extracted using the position of those points. The material properties of these elements will be changed to replicate the corrosion induced cracks on the model. Three sets of analyses will be undertaken here:
   - 3.1. Re-FEM coupled with reference 1D bond-slip relation;
   - 3.2. Re-FEM coupled with shifted/corroded 1D bond-slip relation;
   - 3.3. Re-FEM coupled with bond-corrosion model.
4. **Discrete crack:** Here, the interface elements are used to replicate the approximate path of the dominant crack in the model. A discrete crack model based on the Hordjik tension softening curve [58] is attributed to the interface elements to model the cracked region. Different starting points on the Hordjik curve is used to show the effect of crack opening on the results.

4.1. Experiments

Replication of crack patterns in the FE model needs prior knowledge of the crack pattern and crack width. Berrocal et al. [59] performed a corrosion test on cylinders with a single ϕ16 mm ribbed reinforcing bar at the center, which is stuck out from one of the circular sides, also known as "lollipop" specimens (Figure 4). The authors tested and reported the compressive cube strength, f_{cm}, on 100 mm cubes and the splitting tensile strength, f_{ctm}, on 150 mm cubes. The material properties are shown in Table 2.

Three reference (without corrosion) and three corroded specimens underwent the mechanical pull out test. Accelerated corrosion tests were conducted to reduce the time needed to initiate corrosion induced splitting cracks on the concrete cover. The development of the first crack was monitored and crack paths

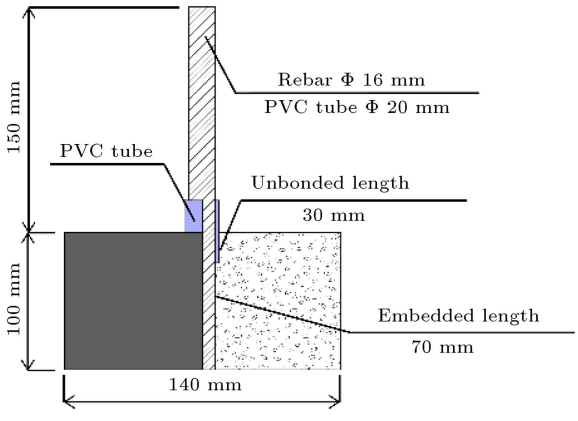

Figure 4. Dimensions of the Lollipop specimen [59].

Table 2. Material properties of concrete [59].

f_{cm} (cube)		f_{ctm}	
Avg.	**Std. dev.**	**Avg.**	**Std. dev.**
56.0 MPa	1.3 MPa	4.2 MPa	0.2 MPa

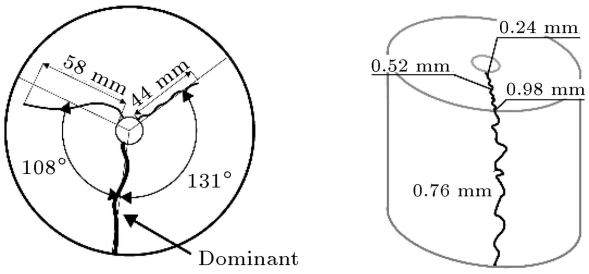

Figure 5. Crack path and crack width due to corrosion of plain concrete specimens with cover to bar ratio of 4.0 [60].

of all visually detectable cracks were investigated and documented for the corroded specimens [60]. Measurement of crack width was just possible for the dominant crack in each specimen. The other cracks were too narrow for a sophisticated measurement. This value was measured and documented on four different points on the path of the crack. Figure 5 shows the crack pattern in the corroded plain concrete specimen with cover to bar ratio of 4.0.

The corrosion level was calculated for each bar using gravimetric steel loss measurements, assuming the measured loss was concentrated on the 70 mm bar length embedded in the concrete. The corrosion level showed an average of 8.43% of steel loss.

Pull-out tests were performed on both reference and corroded specimens. The pull-out force applied to the protruding end of the rebar, along with the passive slip, which is defined as the relative displacement of steel and concrete at the other side of the rebar, was measured. Figure 6 shows the graphs for both the reference and corroded specimens [60]. The curves mentioned by "RefSp#" show the results of the pull-out test on the reference specimens, and the curves mentioned by "CorSp#" show the same results for the corroded ones. The bond capacity on average decreased by 80% after corrosion.

4.2. Finite element model

Finite element models were built by pre-processing tools in the DIANA finite element package [61]. The reported material properties of concrete were converted to data applicable in the DIANA's environment. Thus, the compressive strength of 100 mm cubes and the tensile strength of 150 mm cubes were converted to the corresponding values for a 150 mm cylinder by multiplying them by correction factors, 0.9×0.85 and 0.9, respectively. The fracture energy was derived from MC1990 guidelines [57]. The material properties of steel and concrete are shown in Table 3. Also, to consider the improbable case of yielding of the steel bars, the steel yield strength was used in the model.

Interface elements were also introduced to model the corrosion and bond slip behavior in the concrete-steel interface. There are two main approaches to model the bond-slip behavior and deterioration of bond-slip in DIANA: (1) bond slip as input should be submitted to the program primer for analysis and (2) the bond-slip behavior is calculated during analysis using a subroutine. In this subroutine, the bond slip relationship is not input and it will be derived from the model based on the cover to bar ratio, the material properties, and the amount of corrosion. In both approaches, a uniform corrosion distribution was assumed around the rebar.

The nodes on the bottom surface of the concrete cylinder (Figure 7) were fixed in a vertical direction and displacement was applied on one end of the reinforcement, which is stuck out of the concrete cylinder. The meshing process was performed using 4 mm tetrahedral

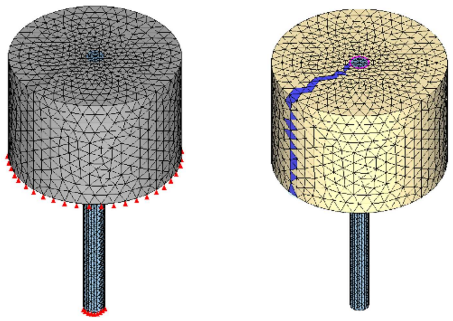

Figure 7. Finite element model of the lollipop specimens (left) and cracked elements (right).

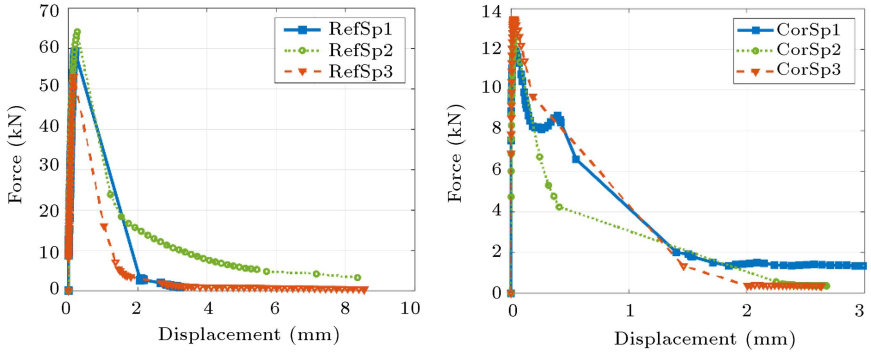

Figure 6. Pull-out force versus passive slip for reference (left) and corroded (right) specimens [60].

Table 3. Material properties of steel and concrete in Finite Element (FE) analysis.

Steel properties		Concrete properties	
Young's modulus	200 GPa	Young's modulus	35.8 GPa
Poisson's ratio	0.3	Poisson's ratio	0.15
Plasticity model	Von Mises	**Total strain-based rotating crack model:**	
Yield strength	535 MPa	Tensile curve, strength	Hordjik [58], 3.76 MPa
		Mode I tensile fracture energy	77 N/m
		Compressive curve, strength	Thorenfeldt [62], 38.7 MPa

elements. Cracked elements were extracted based on the crack path shown in Figure 5. Since the global mesh size was fixed, the crack width did not have any effects on the geometrical extractions of the cracked elements. However, it can be used to justify the strength deterioration of the material, which will be explained in the next section. The final FE model and the extracted crack path are shown in Figure 7.

To validate the model and material properties, specimens under pull-out tests were simulated and the results were compared with the experimental observations. Three characteristics were monitored for validation: (a) load-displacement curves, (2) crack patterns, and (3) failure modes. If there is a good agreement between analysis and experimental results for all three aspects, one can claim that the analysis can describe the experiments reasonably well.

4.2.1. 1D-ARC interface model

The 1D ARC showed a complete pull out failure and wrong force-displacement curve when the bond slip values in the CEB FIP model code [57] were used in the finite element model. Because the purpose of this step was to derive a representative reference model for applying corrosion, the bond-slip curve was extracted from experimental results and used instead of CEB FIP values. The short embedment length justifies the use of the local bond-slip relation. Figure 8(a) and (b) shows the force-displacement curve and principal strain contours for the 1D-ARC approach. The failure mode and crack pattern are not correct, but the force-displacement curve is reasonably accurate. The principal strain was used to monitor crack development. An element is cracked if the strain exceeds 0.001.

Bond corrosion interface model

A bond corrosion model [28] was used for interface elements, keeping all other properties the same as in the 1D ARC case. Figure 8(a) and (c) shows a splitting failure mode and the force-displacement curve is close to the experimental results. In Figure 8(a), 'Simulation bo-co' refers to the results of the simulation using the bond-corrosion interface model.

4.3. Results

The verified FE model is used to simulate the pull-out phase for the corroded specimens. The corrosion

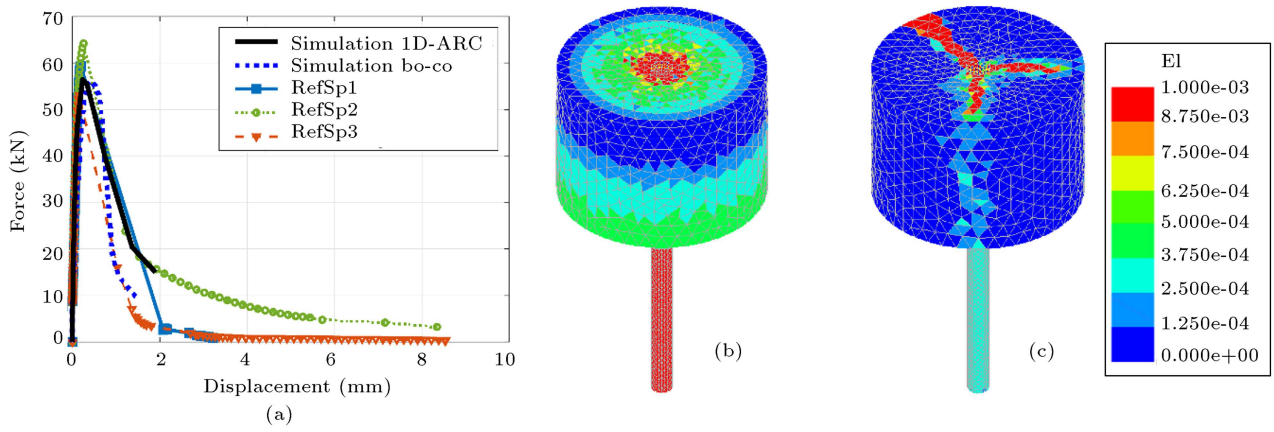

Figure 8. (a) Force-displacement curve of the pull-out test on the reference model. (b) Principal strain in the same analysis using the 1D ARC model for the interface elements. (c) Principal strain in the same analysis using bond-corrosion model for the interface elements.

is applied with different methods as described in the third section of this paper.

1. **Method of adjusted 1D-ARC.** Adjusting the 1D-ARC input based on the level of corrosion deteriorates the bond-slip characteristic of the interface elements. As shown in Figure 9(a) and (b), the model showed a pull out failure, which is in contrast with that observed in the experiments. On the other hand, the force-displacement curve is reasonably accurate. The corrosion penetration for the specimens was about 340 μm.
2. **Method of 3D bond corrosion.** In this approach, a corrosion phase was applied before the mechanical pull out phase. Because the flow of the corrosion has not been implemented in the subroutine, the measured corrosion level cannot be applied in the analysis. The maximum applicable amount of corrosion in the simulation was determined to be around 155 μm. In Figure 9(a) and (c), the splitting failure of the model in the mechanical phase is shown. The force-displacement curve shows a 50% difference between measured pull-out force and the analysis results.
3. **Method of Re-FEM.** In the Re-FEM method, the material properties of the extracted elements, which show the propagation path of the corrosion cracks, were changed. To study the effect of changing material properties, four cases were considered. The Young modulus, the tensile strength, and the fracture energy of all cases were reduced to 85%, 50%, 25%, and 1% of the reference values, respectively. Ideally, a relation between the crack properties and change of material properties could be found based on the experimental data. Changing both the Young modulus and tensile strength simultaneously keeps the crack strain fixed. Deterioration of the bond-slip capacity should be handled separately, since adding the cracked elements does not replicate this effect as well.

   3.1. **Re-FEM + reference 1D-ARC:** Here, Re-FEM is coupled with reference 1D-ARC input. As shown in Figure 10, the force displacement

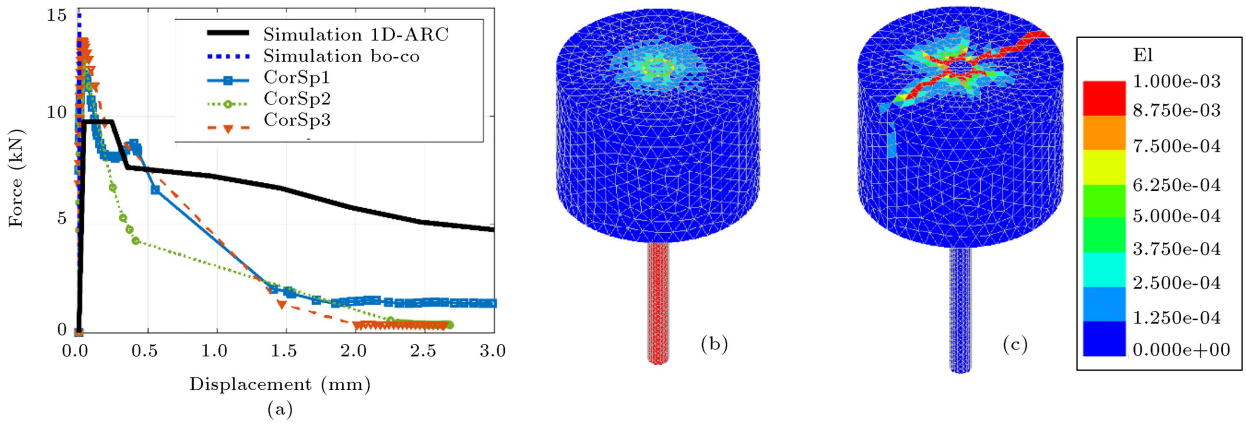

Figure 9. (a) Force-displacement curve of the pull-out test on the corroded model. (b) Principal strain in the same analysis using shifted 1D-ARC method for the interface elements. (c) Principal strain in the same analysis using bond-corrosion model for the interface elements.

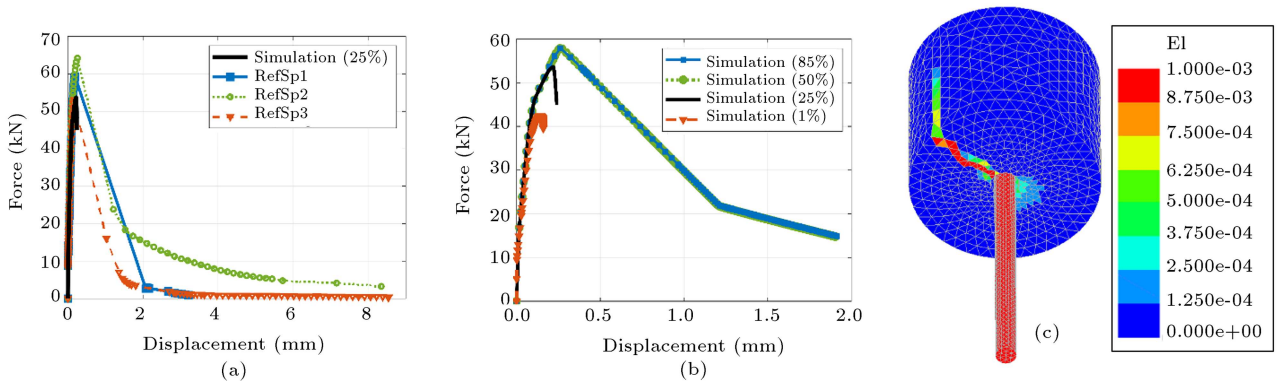

Figure 10. Use of Re-FEM + reference 1D ARC: (a) Comparison of force-displacement curves in the pull-out test, (b) effect of scaling material parameters (young modulus, tensile strength and fracture energy) on the force-displacement curve obtained from the simulation, and (c) principal strain obtained from simulation with scaled material parameter (25%).

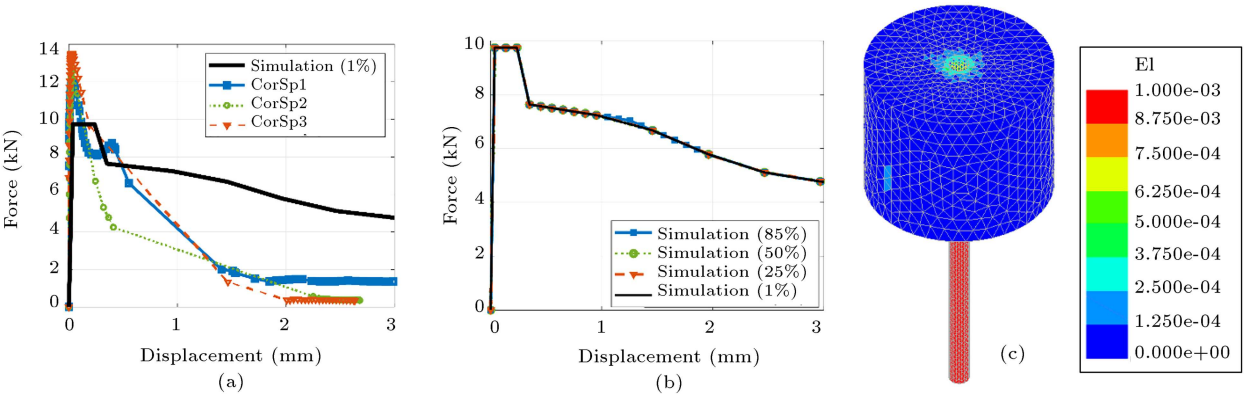

Figure 11. Use of Re-FEM + adjusted 1D ARC: (a) Comparison of force-displacement curves in the pull-out test, (b) effect of scaling material parameters (young modulus, tensile strength and fracture energy) on the force-displacement curve obtained from the simulation, and (c) principal strain obtained from simulation with scaled material parameter (1%).

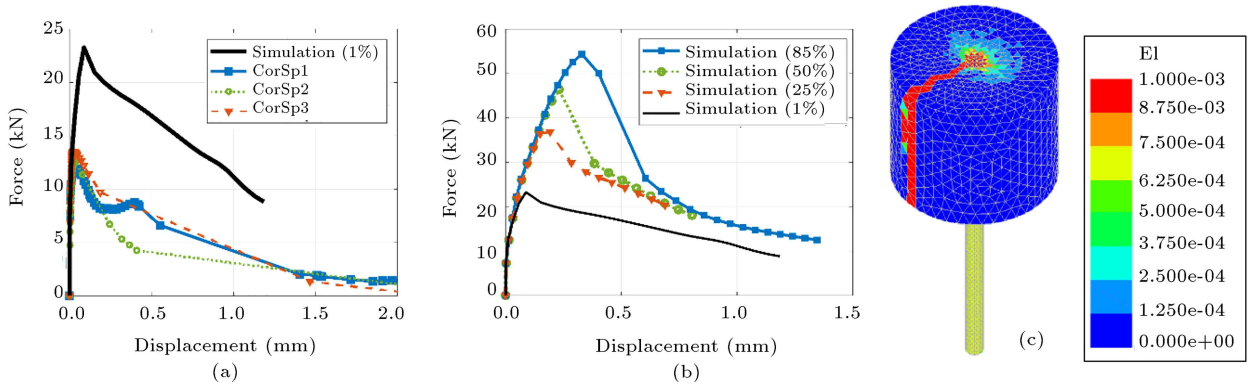

Figure 12. Use of Re-FEM + bond-corrosion: (a) Comparison of force-displacement curves in the pull-out test, (b) effect of scaling material parameters (young modulus, tensile strength and fracture energy) on the force-displacement curve obtained from the simulation, and (c) principal strain obtained from simulation with scaled material parameter (1%).

is not satisfying. Also, while the contour shows the first stages of crack development, the failure mode is splitting failure combined with pull-out, as observed in the experiments;

3.2. **Re-FEM + adjusted 1D-ARC:** As shown in Figure 11, the force-displacement response is not changed by introducing cracked elements into a model with adjusted 1D-ARC input. Therefore, it is obvious that the effects of bond deterioration are significantly higher than crack development in this case. The failure mode is still incorrect;

3.3. **Re-FEM + bond-corrosion:** Figure 12 shows that the crack is developed on the previously specified path. The failure mode is correct here, but the force-displacement result is not close to the experimental observations. Although, the trend in Figure 12(b) is promising.

4. **Method of discrete crack.** Here, instead of changing the element material properties, a layer of interface elements was added along the approximate path of the dominant crack. Then, a model of discrete cracking based on the Hordjik tension softening curve [58] was used for the interface elements to consider the effects of the crack in the model. Different starting points on the Hordjik curve is used to show the influence of crack opening on the results.

4.1. **Discrete crack + reference 1D-ARC:** The generated discrete model was coupled with reference 1D-ARC input. The reference 1D-ARC bond-slip values do not influence the force capacity of the specimens. As shown in Figure 13, the discrete elements also do not have a satisfying influence on the force displacement values, since weakening them has not sufficiently decreased the force capacity of the model. Also, we can observe an opening in the discrete interface, about 0.2 mm, and the contour shows the first stages of crack development on the other side of the

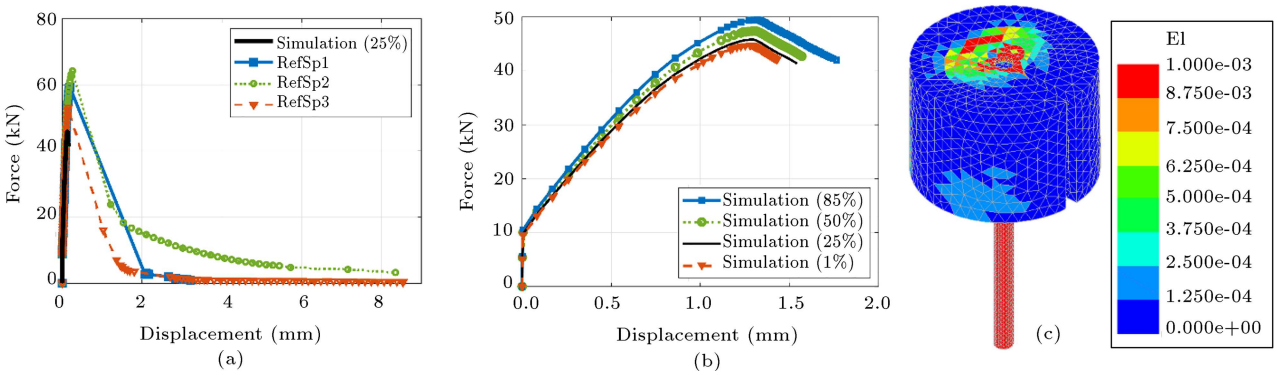

Figure 13. Use of discrete crack + reference 1D ARC: (a) Comparison of force-displacement curves in the pull-out test, (b) effect of scaling material parameters (young modulus, tensile strength and fracture energy) on the force-displacement curve obtained from the simulation, and (c) principal strain obtained from simulation with scaled material parameter (25%).

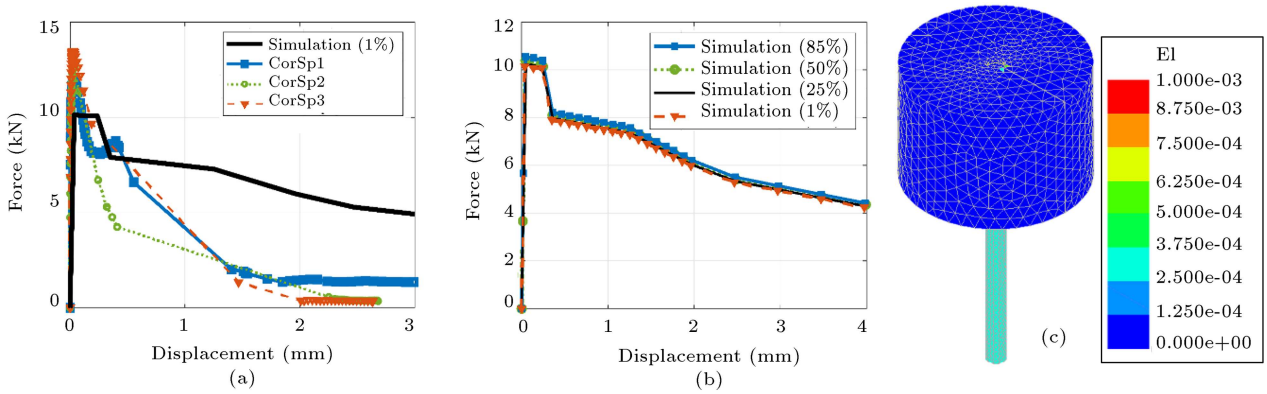

Figure 14. Use of discrete crack + adjusted 1D ARC: (a) Comparison of force-displacement curves in the pull-out test, (b) effect of scaling material parameters (young modulus, tensile strength and fracture energy) on the force-displacement curve obtained from the simulation, and (c) principal strain obtained from simulation with scaled material parameter (1%).

rebar. The failure mode is between pull-out and splitting failure and quite similar to the experiments;

4.2. **Discrete crack + adjusted 1D-ARC:** As observed in the corresponding section for Re FEM, the effect of adjusting the bond-slip behavior has dominated the effect of changing the element's material properties. Here, the same phenomenon is observed and, as shown in Figure 14, the force displacement is not changed by introducing a discrete interface into the model and altering the material properties of the interface. Therefore, the same conclusion is valid here that the effects of bond deterioration are significantly greater than crack development. The failure mode is pull out. The bond-slip is so weak here that the interface elements on the crack path are not opened;

4.3. **Discrete crack + bond-corrosion:** The steel-concrete interface in the model is described by the bond-corrosion subroutine. Figure 15 shows that the force-displacement curve for this case is close to the experimental observations. However, changing the material properties of the discrete interface does not have a significant influence on the overall force capacity of the model. The opening of the interface is about 0.01 mm. The figure also shows that another crack is growing on the other side of the concrete specimen. However, the discrete interface prevents the growth of dominated cracks. The failure mode is splitting, and a significant pull-out of the reinforcement is not observed here. It can be concluded from the results that a discrete surface can assist the bond-corrosion model to reach a better estimation of the force capacity.

5. Summary and conclusion

This paper is aimed at reviewing different approaches for incorporating corrosion-induced cracks in a finite

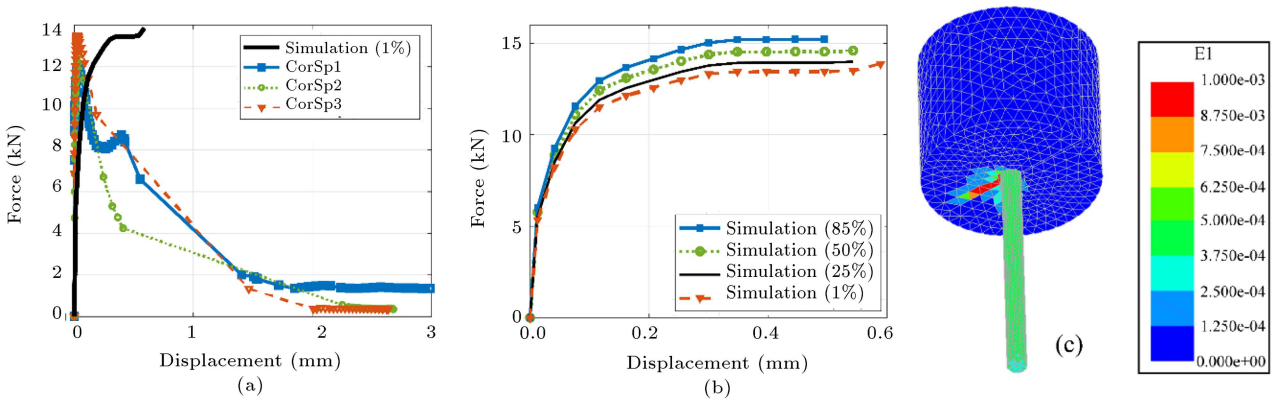

Figure 15. Using discrete crack + bond-corrosion: (a) Comparison of force-displacement curves in the pull-out test, (b) effect of scaling material parameters (young modulus, tensile strength and fracture energy) on the force-displacement curve obtained from the simulation, and (c) principal strain obtained from simulation with scaled material parameter (1%).

Table 4. Comparison of finite element models for corrosion-induced cracking.

Models	Advantages	Disadvantages
Smeared crack models	• Showing dominant and non dominant cracks • No prior knowledge of the crack path before the simulation • Can change the crack propagation direction based on the formulation	• High computational cost
Discrete crack models	• Low computational cost (if the crack path is known)	• Mesh bias • High computational cost upon re meshing • Crack propagates in a defined path • Just shows dominant cracks
Sequentially linear analysis	• Fewer convergence problems • Suitable for symmetric loading	• Not suitable for non-proportional loading • Inability to model crack closure • Not implemented in commercial software • Cannot be included in a phased analysis
Embedded crack approaches	• Crack geometry independent of mesh boundaries • No need for re meshing	• Stress locking • Geometric continuity might be damaged and should be saved by crack tracking procedures
XFEM	• Crack geometry independent of mesh boundaries • Little or no need for re meshing • Good numerical robustness	• Implementation needs a great effort

element model of a reinforced concrete structure. In the first section, different crack models were presented and discussed based on their advantages and disadvantages. Table 4 summarizes the points mentioned previously.

In addition to the crack models, two common approaches for inclusion of corrosion phenomena into the finite element analysis were explained in detail:

- **1D-ARC interface model:** This model is easy to use and simulates the corrosion and the change in bond-slip properties of the structure using experimental input data. While this model shows the load response and capacity of the structure with high accuracy, the failure mode might not be exact.
- **Bond corrosion interface model:** This model is not as straight-forward as the 1D ARC approach. The interface elements should be defined between concrete and steel and the corrosion is updated in each iteration. This model predicts both the capacity of the structure and the failure mode with good accuracy. However, the computational cost of this approach is significantly higher.

Entering experimental observation by changing the properties of elements on the crack path, based

on the crack-width and amount of corrosion, can be a suitable method to enter the information obtained from experiments into the FE analysis and use them for further assessment and maintenance decisions.

A finite element model was used to study the efficacy of different corrosion models for reinforced concrete. Results showed that the 1D-ARC model delivers a promising force displacement output, but the failure mode was incorrect. It is an expected deficiency because 1D ARC had been introduced to produce a rough approximation of the bond capacity of the structure. Using the bond corrosion model, the force displacement response was accurate until the point of maximum force, but the analysis diverged after that point. Also, the failure mode was correct because this approach always considers confinement changes after the corrosion.

This paper introduces a new method for adding cracked elements to the FE model named Re-FEM. Using this method, the force displacement response for the corroded specimens was overestimated about 70% but showed a correct trend. The failure mode and crack pattern were correct because the model considers the confinement changes as well as dominant cracks. Moreover, the analysis continued after the peak point in the force-displacement curve and made it possible to monitor the behavior of the specimen in the softening regime.

A set of interface elements with discrete-cracking behavior was added to the original model to study the features of the discrete-cracking approach. When this model was coupled with a bond corrosion model for the steel- concrete interface, very promising results for the force displacement behavior of the model were achieved, which showed a pretty similar peak load. However, changing the material properties of the discrete interface did not have a significant influence on the force capacity of the whole model. Notwithstanding these features, further developments are required to justify the correct amount of material deterioration due to cracking and modify the overestimation in each case.

Acknowledgements

This research was funded by TABAN Science Program and hosted by the RISE Research Institutes of Sweden (formerly named The Swedish Cement and Concrete Research Institute). The authors also acknowledge the support from the University of Tehran.

References

1. COST 345 "Procedures required for assessing highway structures. Working Group 1 report on the current stock of highway structures in European countries, the cost of their replacement and the annual cost of maintaining, repairing and renewing them", TRL Limited, Crowthorne, UK (2004).
2. Zandi, K., Flansbjer, M., Johansson, M., Fahimi, S., Spetz, J., Raña, I.V., and Boubitsas, D., *Autonomous Automated Non-Intrusive Condition Assessment - UNICA*, RISE CBI Swedish Cement and Concrete Research Institute (2017).
3. Shahsavari, H., Baghani, M., Sohrabpour, S., and Naghdabadi, R. "Continuum damage-healing constitutive modeling for concrete materials through stress spectral decomposition", *International Journal of Damage Mechanics*, **25**(6), pp. 900–918 (2015).
4. Shahsavari, H., Naghdabadi, R., Baghani, M., and Sohrabpour, S. "A finite deformation viscoelastic-viscoplastic constitutive model for self-healing materials", *Smart Materials and Structures*, **25**(12), p. 125027 (2016).
5. Shahsavari, H., Baghani, M., Naghdabadi, R., and Sohrabpour, S. "A thermodynamically consistent viscoelastic-viscoplastic constitutive model for self-healing materials", *Journal of Intelligent Material Systems and Structures*, **29**(6), pp. 1065–1080 (2017).
6. Oucif, C. and Mauludin, L.M. "Continuum damage-healing and super healing mechanics in brittle materials: A state-of-the-art review", *Applied Sciences*, **8**(12), p. 2350 (2018).
7. Dolatabadi, R., Mohammadi, A., and Baghani, M. "A computational simulation of electromembrane extraction based on Poisson-Nernst-Planck equations", *Analytica Chimica Acta*, **1158**, p. 338414 (2021).
8. Altun, F. and Dandin, Z. "Experimental investigation into steel ber addition to reinforced concrete cantilever beams under a cyclic load effect", *Scientia Iranica*, **21**(6), pp. 1743–1749 (2014).
9. Mehrpay, S. and Saleh-jalali, R. "Strain rate effect in the mesoscopic modeling of high-strength steel fiber-reinforced concrete", *Scientia Iranica*, **24**(2), pp. 512–525 (2017).
10. Song, Y., Wightman, E., Tian, Y., Jack, K., Li, X., Zhong, H., Bond, P.L., Yuan, Z., and Jiang, G. "Corrosion of reinforcing steel in concrete sewers", *Science of The Total Environment*, **649**, pp. 739–748 (2019).
11. Shahsavari, H., Naghdabadi, R., Baghani, M., and Sohrabpour, S. "A viscoelastic-viscoplastic constitutive model considering damage evolution for time dependent materials: Application to asphalt mixes", *International Journal of Damage Mechanics*, **25**(7), pp. 921–942 (2016).
12. Shojaeifard, M., Baghani, M., and Shahsavari, H. "Rutting investigation of asphalt pavement subjected to moving cyclic loads: An implicit viscoelastic-viscoplastic-viscodamage FE framework", *International Journal of Pavement Engineering*, **21**(11), pp. 1393–1407 (2020).
13. Bell, B., *European Railway Bridge Problems*, Sustainable Bridges project deliverable D1.3. Available at: www.sustainablebridges.net/WPI (2004).

14. Andrade, C., Alonso, C., and Molina, F.J. "Cover cracking as a function of bar corrosion.1. experimental test", *Materials and Structures*, **26**(162), pp. 453–464 (1993).

15. *Bond of Reinforcement in Concrete*, State-of-Art report, fib Fédération internationale du béton, prepared by Task Group Bond Models, Lausanne, p. 427 (2000).

16. Lundgren, K. "Effect of corrosion on the bond between steel and concrete: An overview", *Magazine of Concrete Research*, **59**(6), pp. 447–461 (2007).

17. Sæther, I. "Bond deterioration of corroded steel bars in concrete", *Structure and Infrastructure Engineering*, **7**(6), pp. 415–429 (2011).

18. Coronelli, D., Hanjari, K.Z., Lundgren, K., and Rossi, E. "Severely corroded reinforced concrete with cover cracking: Part 1. Crack initiation and propagation", in *Modelling of Corroding Concrete Structures*, Springer, Dordrecht, pp. 195–205 (2011).

19. Zandi, K., *Structural Behaviour of Deteriorated Concrete Structures*, in Department of Civil and Environmental Engineering, Chalmers University of Technology (2010).

20. Regan, P.E. and Kennedy Reid, I. "Assessment of concrete structures affected by delamination: 1 - Effect of bond loss", *Studies and Research - Annual Review of Structural Concrete*, **29**, pp. 245–275 (2009).

21. Higgins, C. and Farrow III, W.C. "Tests of reinforced concrete beams with corrosion-damaged stirrups", *Aci Structural Journal*, **103**(1), pp. 133–141 (2006).

22. Lundgren, K., Kettil, P., Zandi, K., Schlune, H., and Roman, A.S.S. "Analytical model for the bond-slip behaviour of corroded ribbed reinforcement", *Structure and Infrastructure Engineering*, **8**(2), pp. 157–169 (2012).

23. Coronelli, D. and Gambarova, P. "Structural assessment of corroded reinforced concrete beams: Modeling guidelines", *Journal of Structural Engineering*, **130**(8), p. 1214 (2004).

24. Zandi, K., Kettil, P., and Lundgren, K. "Analysis of mechanical behavior of corroded reinforced concrete structures", *ACI Structural Journal*, **108**(5), pp. 532–541 (2011).

25. Lundgren, K. "Bond between ribbed bars and concrete. Part 1: Modified model", *Magazine of Concrete Research*, **57**(7), pp. 371–382 (2005).

26. Lundgren, K. "Bond between ribbed bars and concrete. Part 2: The effect of corrosion", *Magazine of Concrete Research*, **57**(7), pp. 383–395 (2005).

27. Zandi Hanjari, K., Lundgren, K., Plos, M., and Coronelli, D. "Three-dimensional modelling of structural effects of corroding steel reinforcement in concrete", *Structure and Infrastructure Engineering*, **9**(7), pp. 702–718 (2013).

28. Lundgren, K. "Bond between ribbed bars and concrete. Part 2: The effect of corrosion", *Magazine of Concrete Research*, **57**(7), pp. 383–396 (2005).

29. Borst, R.D., Remmers, J.J., Needleman, A., and Abellan, M.A. "Discrete vs smeared crack models for concrete fracture: bridging the gap", *International Journal for Numerical and Analytical Methods in Geomechanics*, **28**(78), pp. 583–607 (2004).

30. DeJong, M.J., Hendriks, M.A.N., and Rots, J.G. "Sequentially linear analysis of fracture under nonproportional loading", *Engineering Fracture Mechanics*, **75**(18), pp. 5042–5056 (2008).

31. Jirásek, M. and Belytschko. T. "Computational resolution of strong discontinuities", in *Proceedings of Fifth World Congress on Computational Mechanics*, WCCM V, Vienna University of Technology, Austria (2002).

32. Van Mier, J.G., *Fracture Processes of Concrete*, **12**, CRC press (1996).

33. De Borst, R. "Smeared cracking, plasticity, creep, and thermal loading-A unified approach", *Computer Methods in Applied Mechanics and Engineering*, **62**(1), pp. 89–110 (1987).

34. Feenstra, P.H., Rots, J.G., Arnesen, A., Teigen, J.G., and Hoiseth, K.V. "A 3D constitutive model for concrete based on a co-rotational concept", *Computational Modelling of Concrete Structure, Proceedings of the Euro-C 1998 Conference on Computational Modelling of Concrete Structures*, Badgastein, Austria, pp. 13–22 (1998).

35. Feenstra, P.H. and De Borst, R. "A composite plasticity model for concrete", *International Journal of Solids and Structures*, **33**(5), pp. 707–730 (1996).

36. Ngo, D. and Scordelis, A. "Finite element analysis of reinforced concrete beams", in *ACI Journal Proceedings, ACI*, **64**(3), pp. 152–163 (1967).

37. Stankowski, T., Runesson, K., and Sture, S. "Fracture and slip of interfaces in cementitious composites. I: Characteristics", *Journal of Engineering Mechanics*, **119**(2), pp. 292–314 (1993).

38. Rots, J. "Sequentially linear continuum model for concrete fracture", *Fracture Mechanics of Concrete Structures*, **2**, pp. 831–840 (2001).

39. Rots, J.G. and Invernizzi, S. "Regularized sequentially linear saw-tooth softening model", *International Journal for Numerical and Analytical Methods in Geomechanics*, **28**(78), pp. 821–856 (2004).

40. Barros, H., Hendriks, M.A.N., and Rots, J.G. "Sequentially linear versus nonlinear analysis of RC structures", *Engineering Computations*, **30**(6), pp. 792–801 (2013).

41. Eliáš, J., Frantík, P., and Vořechovský, M. "Improved sequentially linear solution procedure", *Engineering Fracture Mechanics*, **77**(12), pp. 2263–2276 (2010).

42. Reyes, E., Gálvez, J.C., Cendón, D.A., et al. "An embedded cohesive crack model for finite element analysis of mixed mode fracture of brickwork masonry", in *Computational Plasticity - Fundamentals and Applications, COMPLAS IX*, **29**(12), pp. 1056–1065 (2007).

43. Oliver, J., Huespe, A.E., Samaniego, E., and Chaves, E.W.V. "On strategies for tracking strong discontinuities in computational failure mechanics", in *Fifth World Congress on Computational Mechanics* (2002).

44. Feist, C. and Hofstetter, G. "An embedded strong discontinuity model for cracking of plain concrete", *Computer Methods in Applied Mechanics and Engineering*, **195**(52), pp. 7115–7138 (2006).

45. Sánchez, P.J., Oliver, J., Huespe, A.E., and Sonzogni, V.E. "Finite elements with embedded strong discontinuities for the numerical simulation in failure mechanics: E-Fem and X-Fem", *Mecánica Computacional*, **24**(3), pp. 541–566 (2006).

46. Bhargava, K., Ghosh, A.K., Mori, Y., and Ramanujam, S. "Model for cover cracking due to rebar corrosion in RC structures", *Engineering Structures*, **28**(8), pp. 1093–1109 (2006).

47. Bhargava, K., Ghosh, A.K., Mori, Y., and Ramanujam, S. "Modeling of time to corrosion-induced cover cracking in reinforced concrete structures", *Cement and Concrete Research*, **35**(11), pp. 2203–2218 (2005).

48. Wang, L., Dai, L., Bian, H., Ma, Y., and Zhang, J. "Concrete cracking prediction under combined prestress and strand corrosion", *Structure and Infrastructure Engineering*, **15**(3), pp. 285–295 (2019).

49. Li, C.-Q., Melchers, R.E., and Zheng, J.-J. "Analytical model for corrosion-induced crack width in reinforced concrete structures", *ACI Structural Journal*, **103**(4), p. 479 (2006).

50. Val, D.V., Chernin, L., and Stewart, M.G. "Experimental and numerical investigation of corrosion-induced cover cracking in reinforced concrete structures", *Journal of Structural Engineering*, **135**(4), pp. 376–385 (2009).

51. Richard, B., Ragueneau, F., Cremona, C., Adelaide, L., and Tailhan, J.L. "A three-dimensional steel/concrete interface model including corrosion effects", *Engineering Fracture Mechanics*, **77**(6), pp. 951–973 (2010).

52. Guzmán, S., Gálvez, J.C., and Sancho, J.M. "Modelling of corrosion-induced cover cracking in reinforced concrete by an embedded cohesive crack finite element", *Engineering Fracture Mechanics*, **93**, pp. 92–107 (2012).

53. Chen, E. and Leung, C.K.Y. "Mechanical aspects of simulating crack propagation in concrete under steel corrosion", *Construction and Building Materials*, **191**, pp. 165–175 (2018).

54. Yang, S., Xi, X., Li, K., and Li, C.Q. "Numerical modeling of nonuniform corrosion-induced concrete crack width", *Journal of Structural Engineering*, **144**(8), p. 04018120 (2018).

55. Mak, M.W.T., Desnerck, P., and Lees, J.M. "Corrosion-induced cracking and bond strength in reinforced concrete", *Construction and Building Materials*, **208**, pp. 228–241 (2019).

56. Guzmán, S. and Gálvez, J.C. "Modelling of concrete cover cracking due to non-uniform corrosion of reinforcing steel", *Construction and Building Materials*, **155**, pp. 1063–1071 (2017).

57. Code, CEB-FIP Model "Comité euro-international du béton", *Bulletin d'information*, **213**, p. 214 (1993).

58. Cornelissen, H., Hordijk, D., and Reinhardt, H. "Experimental determination of crack softening characteristics of normal weight and lightweight concrete", *Heron*, **31**(2), pp. 45–46 (1986).

59. Berrocal, C.G., Fernandez, I., Lundgren, K., and Löfgren, I. "Influence of fibre reinforcement on the initiation of corrosion-induced cracks", *Service Life of Cement-Based Materials and Structures*, **1**, pp. 231–240 (2016).

60. Berrocal, C.G., Fernandez, I., Lundgren, K., and Löfgren, I. "Corrosion-induced cracking and bond behaviour of corroded reinforcement bars in SFRC", *Composites Part B: Engineering*, **113**, pp. 123–137 (2017).

61. Diana, T.N.O., *Diana Finite Element Analysis User's Manual Release 10.0*, Delft, The Netherlands (2012).

62. Thorenfeldt, E. "Mechanical properties of high-strength concrete and applications in design", in *Symposium Proceedings, Utilization of High-Strength Concrete*, Norway (1987).

Biographies

Shayan Fahimi received his BS (2014) and MS degrees (2017) in Mechanical Engineering from the University of Tehran, Iran. He is currently a PhD candidate in Structural Engineering at the University of British Columbia. His research interests include nonlinear finite element methods, mechanics of composite materials, poroelasticity, and process modeling.

Mohammad Reza Zakerzadeh received his BS, MS, and PhD degrees in Mechanical Engineering from Sharif University of Technology, Tehran, Iran, in 2002, 2005 and 2012, respectively. He is currently Associate Professor in the School of Mechanical Engineering at the University of Tehran. His research activities include smart material and structures, Shape Memory Alloy (SMA), dynamics, control and robotics.

Mostafa Baghani received his BS degree in Mechanical Engineering from the University of Tehran

in 2006 and his MS and PhD degrees in Mechanical Engineering from Sharif University of Technology, Tehran, Iran, in 2008 and 2012, respectively. He is currently Assistant Professor in the School of Mechanical Engineering at the University of Tehran. His research interests include solid mechanics, nonlinear finite element method, and shape-memory materials constitutive modeling.

Kamyab Zandi received his MS degree in Civil Engineering (2006) and PhD degree in Structural Engineering (2010) at Chalmers University of Technology, Sweden. He is currently Associate Professor at Chalmers University of Technology in Structural Engineering, and a Visiting Professor at Stanford University in Aeronautics & Astronautics. He is also the Director and Principal Investigator of the Digital Twins Lab. His research interests span over several aspects of digital twin, namely, engineering of aerial vehicle platforms equipped with sensors for data collection from infrastructures, data analysis leveraging big data analytics for damage detection, and advanced large-scale FE simulations for condition assessment and service life prediction.